SLOT COUPLED PATCH ANTENNAS

Linda Katehi, Nihad I. Dib, J-C Cheng

December 1993

Slot Coupled Patch Antennas

Linda Katehi

A report prepared for Texas Instruments

Participating Scientists:

Nihad I. Dib, Research Scientist, Ph.D.

J-C Cheng, Graduate Student

Brief Report

During the past few months we concentrated on the characterization of patches which are electromagnetically coupled to their feeding lines. The excitation line can be of stripline, microstrip or coplanar waveguide form printed on the other side of the substrate. A schematic of this geometry is shown on Figure 1. A characteristic of this structure is that the patch may be backed by a cavity as shown in the Figure. The presence of the cavity requires the use of versatile discretization techniques as the integral equation/finite element method in frequency domain or the finite difference method in time domain. In this effort we chose to use both of the above techniques in order to gain some understanding of their capabilities and computer efficiencies in solving this type of problems. As a carriage of our experiment we chose the geometry of a microstrip patch excited by a coplanar waveguide feed through a slot aperture printed on the ground (see Figure 2). This is one of the possible geometries among the electromagnetically coupled patches.

This problem has been approached with two different techniques: (a) The Finite Difference Time Domain Method, (b) the Finite Element/Integral Equation Method. The finite difference time domain method discretizes in a volume, which surrounds the antenna and the feeding line and is bounded by superabsorbing boundary conditions to simulate free-space. A description of this method is given in Appendix A. The FDTD codes used for the derivation of these data have been validated very thoroughly through numerous examples [1]-[4]. The integral equation/

finite element method applies the finite element method inside the cavity and the integral equation outside, above the patch and below the coupling slot. A detailed description of the method is given in Appendix B.

Figures 4 and 5 show the FDTD results for the magnitude and phase of S_{11} as a function of the frequency for the patch with and without the cavity. The dimensions for the patch with the cavity present are given on Figure 3. The cavity has the following dimensions (see Figure 3):

$$D_c = d_p$$
$$W_c = W_p + 2d_p$$
$$L_c = L_p + 2d_p$$

where, D_c is the depth, W_c the width and L_c the length of the cavity. As shown by these results, the effect of the cavity on the performance of the patch is rather minor. This is due to the fact that the dielectric substrate on which the patch is printed is very thin, thus, minimizing the excitation of surface waves. As a result, the addition of the cavity does not disturb the fields excited under the patch. It is expected that thicker substrates will intensify cavity effects. At the present time we try to generate data for thicker substrates where the cavity effects are expected to be more noticeable.

Figure 6 shows a comparison between the FDTD and the integral equation part of the hybrid FEM/IE for the case of the patch without the cavity. As we see, there is a discrepancy at the resonance of the antenna which, we believe, is due to insufficient discretization on the patch as applied by the integral equation method. In fact, only one basis has been considered on the patch as suggested by Pozar in the literature. However, the results show some discrepancies which can be eliminated if a better discretization is considered. The hybrid FEM/IE has been applied to the cavity-backed patch problem but the results have not converged adequately to the right values. At the present time, we are in the process of studying the effects of a number of parameters on convergence. Some of these parameters are the finite element meshing in the cavity and the integral equation discretization of the conductors in the outside region. Preliminary results are encouraging and indicative that we should be able to improve convergence and derive accurate solutions during the next few months.

While we were trying to analyze the geometry of Figure 3 we were able to make the following interesting observations:

FDTD

- The finite difference time domain method was found much easier to implement and use.
- The method requires a lot of memory in view of the space discretization and the time stepping. With the appropriate use of diakoptics, however, the memory requirements should be minimized as the absorbing boundaries can be brought very close to the antenna and feeding line.
- The major advantage of the method is that it can generate, with one run, any desired number of frequency points. This is very important for narrow band antennas where a very dense frequency sampling is required and for wide frequency-band applications where many frequency points are required to cover the desired frequency range.

Hybrid FEM

- The implementation of the method is rather complex.
- The hybrid FEM requires much less memory than the FDTD, but it can only provide one frequency point per run.
- In view of the combination between IE and FEM, the technique is more sensitive to meshing and the relative sizes of the sub-elements created by the FEM and Integral Equation.

The finite difference time domain programs are available for use and can be transferred to Texas Instruments. As it has been discussed, these programs will bet sent electronically, while at the same time a description on how to access and run the programs will be mailed to TI.

Furthermore, we would like to run any other cases which are of interest to TI or for which experimental data may be available.

References

1. J-G. Yook, N.I. Dib, and L.P.B. Katehi, "Time and Frequency Domain Characterization of High-Frequency Interconnections," submitted to *IEEE Transactions on Microwave Theory and Techniques*, special issue on Packaging and Interconnects.
2. N.I. Dib and L.P.B. Katehi, "Analysis of a Transition from a Rectangular Waveguide to a Shielded Dielectric Image Guide Using a Finite Difference Time Domain Method," *IEEE Guided Wave Letters*, Vol.3, Number 9, September, 1993, pp. 327-330.

3. Nihad I. Dib and Linda P.B. Katehi, "Sub-mm Wave Circuit Characterization Using the Finite Difference Time Domain Method," submitted to the Special Issue of the International Journal on Numerical Modelling on The Discrete Time Domain Modeling of Electromagnetic Fields and Networks.
4. N.I. Dib, C-J. Cheng and L.P.B. Katehi, "Characterization of Cavity-Backed Patches Using Frequency and Time-Domain Techniques", submitted for presentation in the 1994 IEEE Antennas and Propagation Society.

FIGURE 1. Slot Coupled Patch Antennas

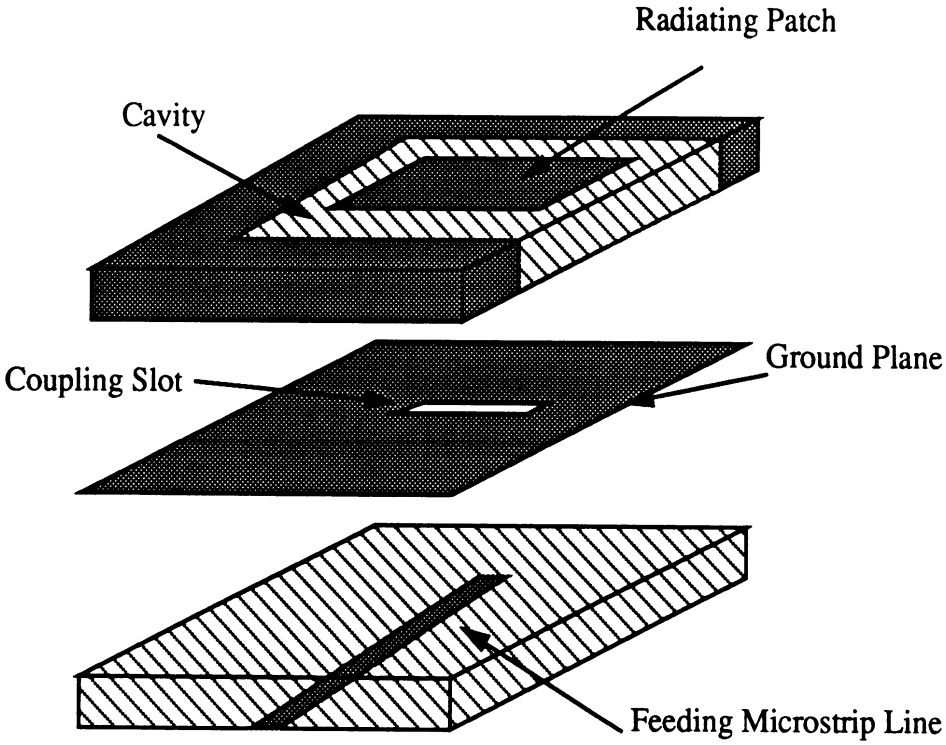

FIGURE 2. A Microstrip Patch Electromagnetically Coupled to a Coplanar Waveguide

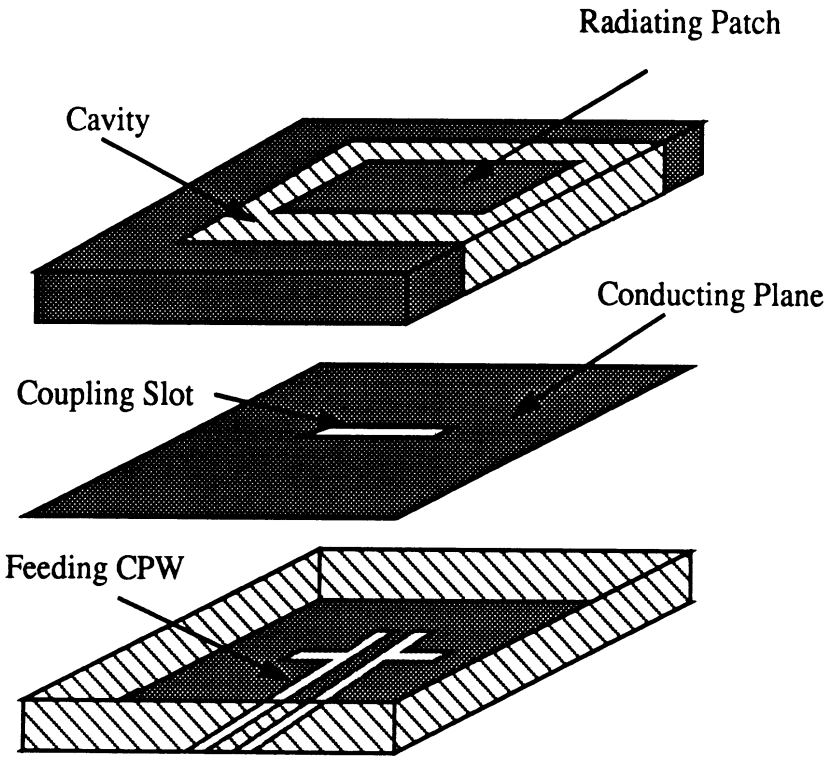

FIGURE 3. Dimensions of the Slot-Coupled Patch.

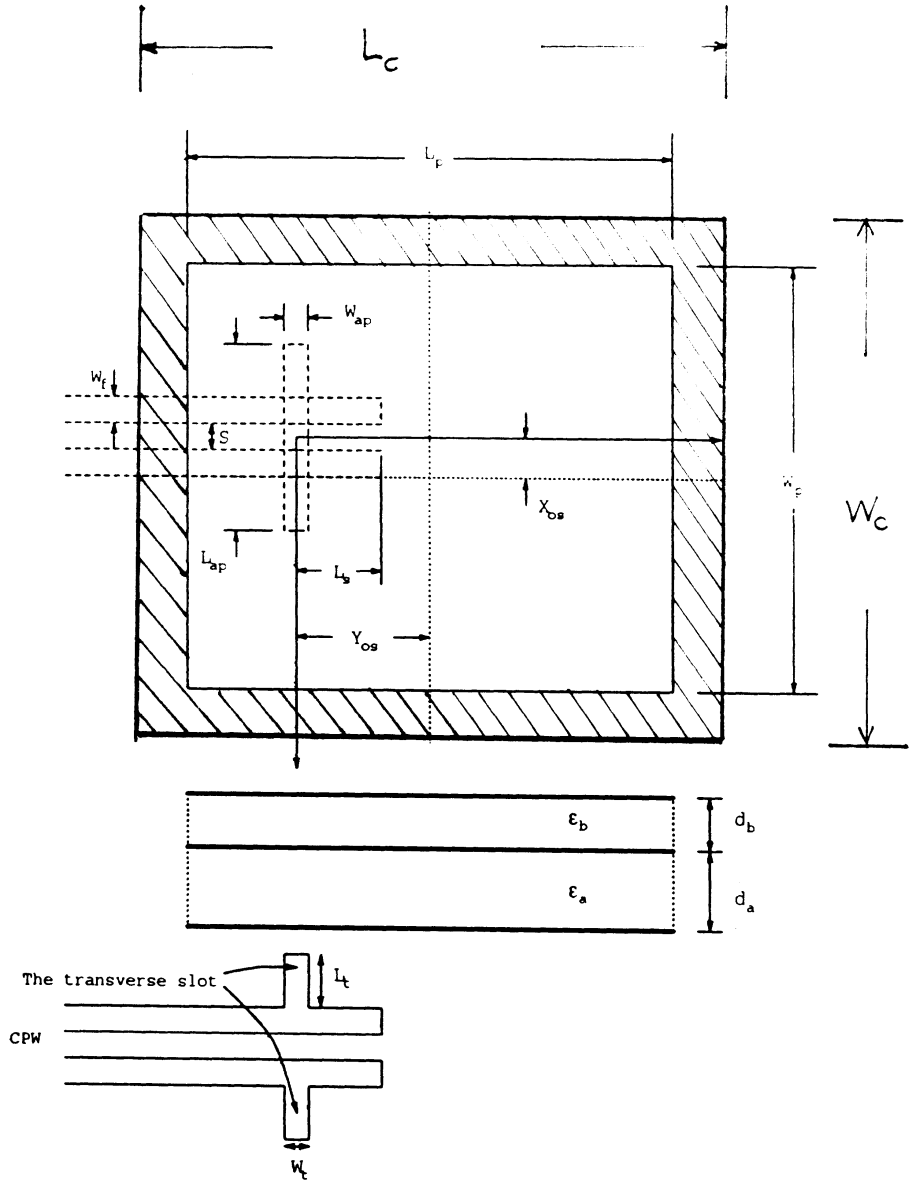

The schematic of the original problem. L_p=7.6mm, W_p=11.4mm, W_{ap}=0.254mm, L_{ap}=6.91mm, W_f=0.254mm, S=0.762mm, L_s=6.858mm, L_t=2.794mm, W_t=0.762mm, X_{os}=0, Y_{os}=0, d_a=0.508mm, d_b=0.254mm, ϵ_a=2.2, ϵ_b=2.2.

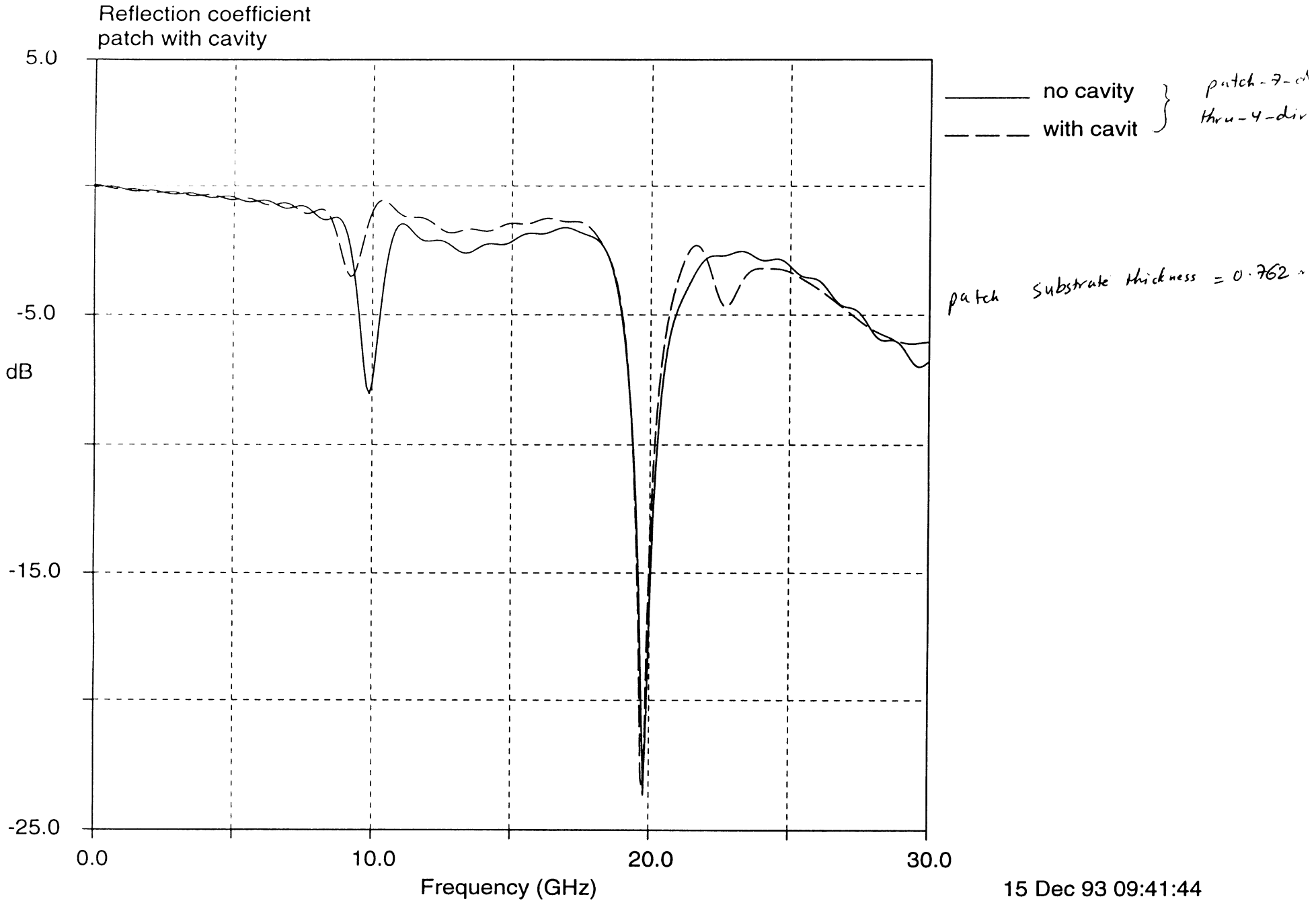
Reflection coefficient
patch with cavity
5.0
-5.0
-15.0
-25.0
dB
0.0
10.0
20.0
30.0
Frequency (GHz)
no cavity
with cavit
15 Dec 93 09:41:44

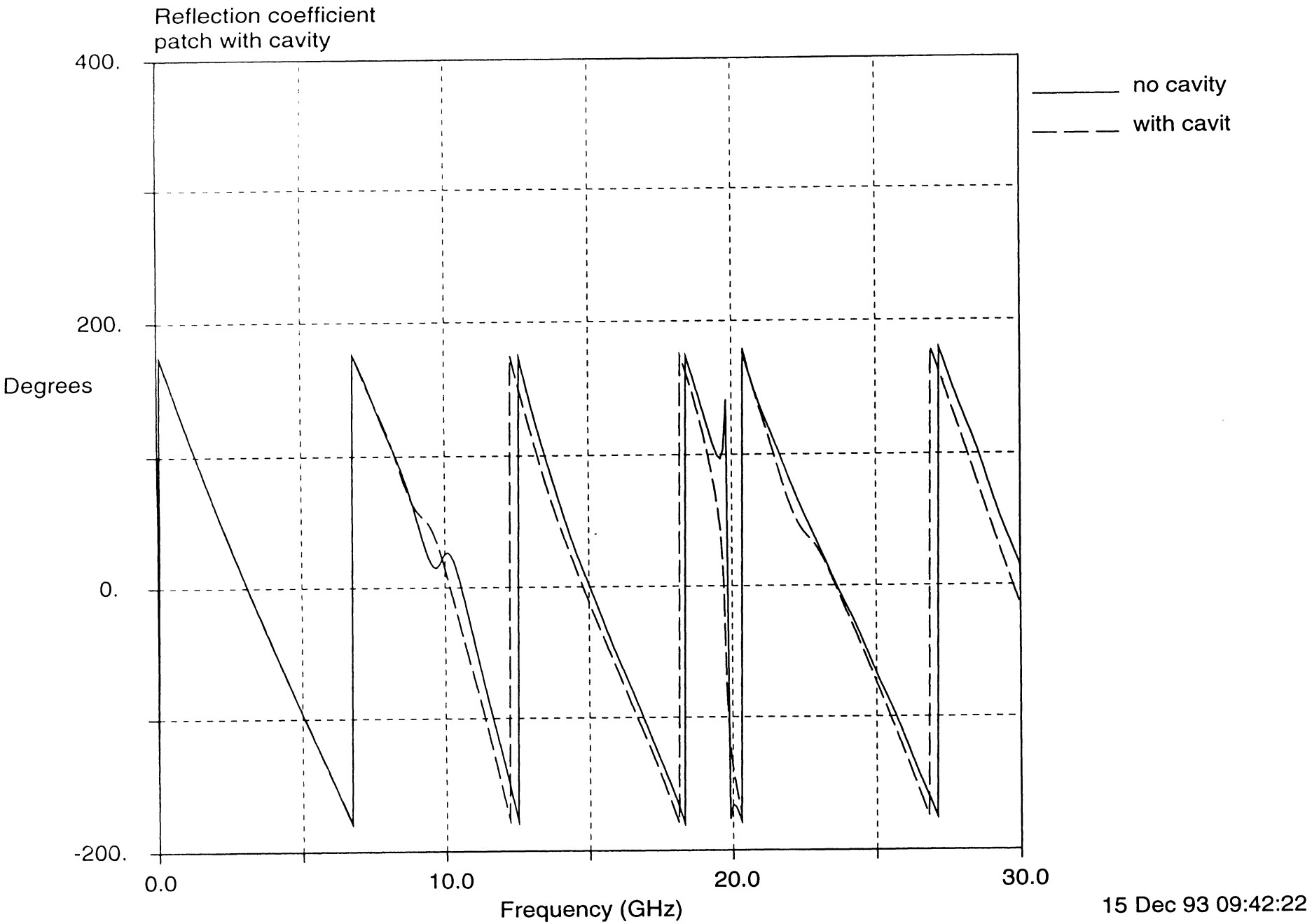
Reflection coefficient
patch with cavity
400.
200.
0.
-200.
Degrees
0.0
10.0
20.0
30.0
Frequency (GHz)
no cavity
with cavit
15 Dec 93 09:42:22

FIGURE 4. Magnitude of S11 for the Geometry of Figure 2 with and without the cavity.

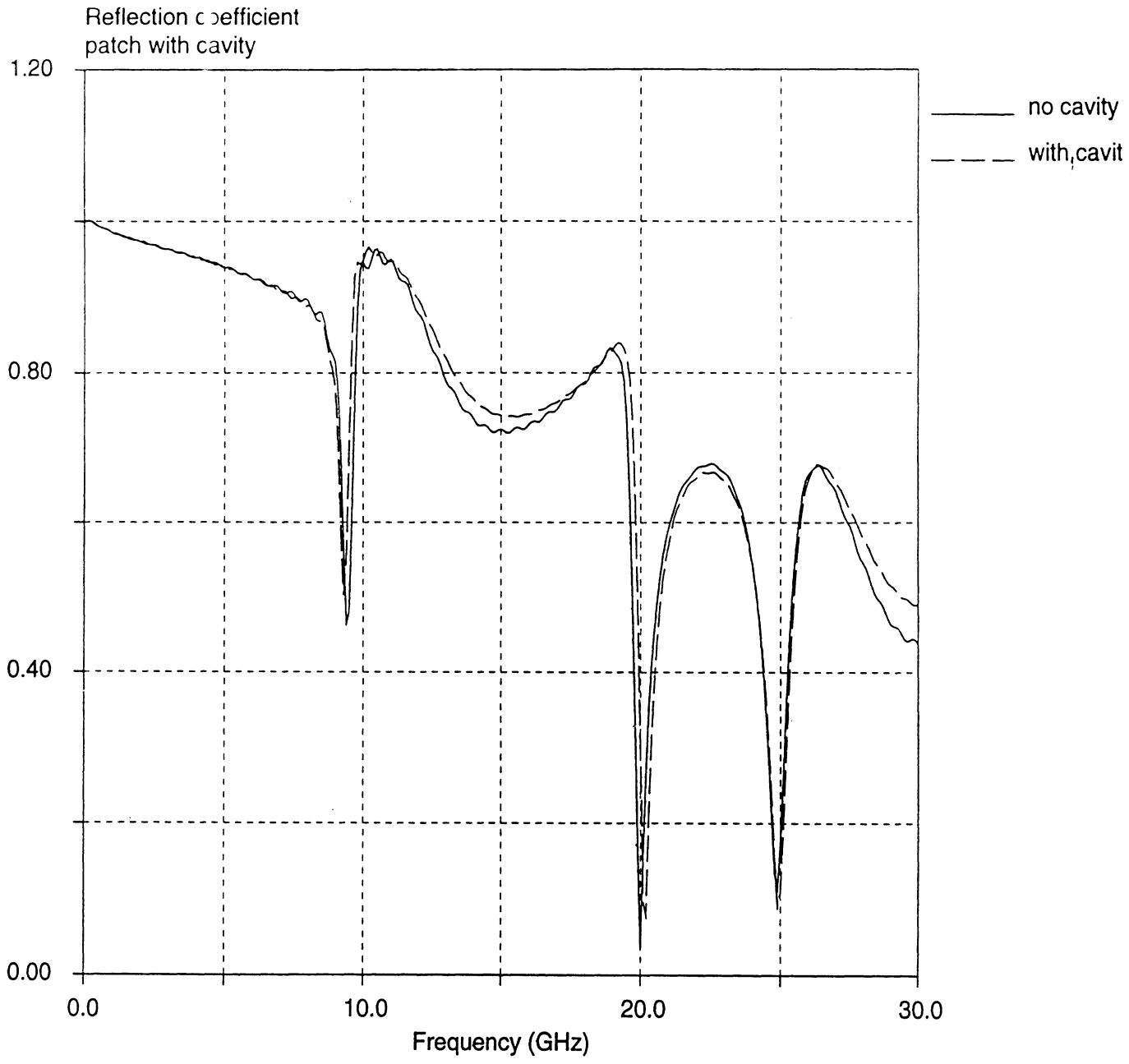

FIGURE 5. Phase of S11 for the Geometry of Figure 2 with and without the cavity.

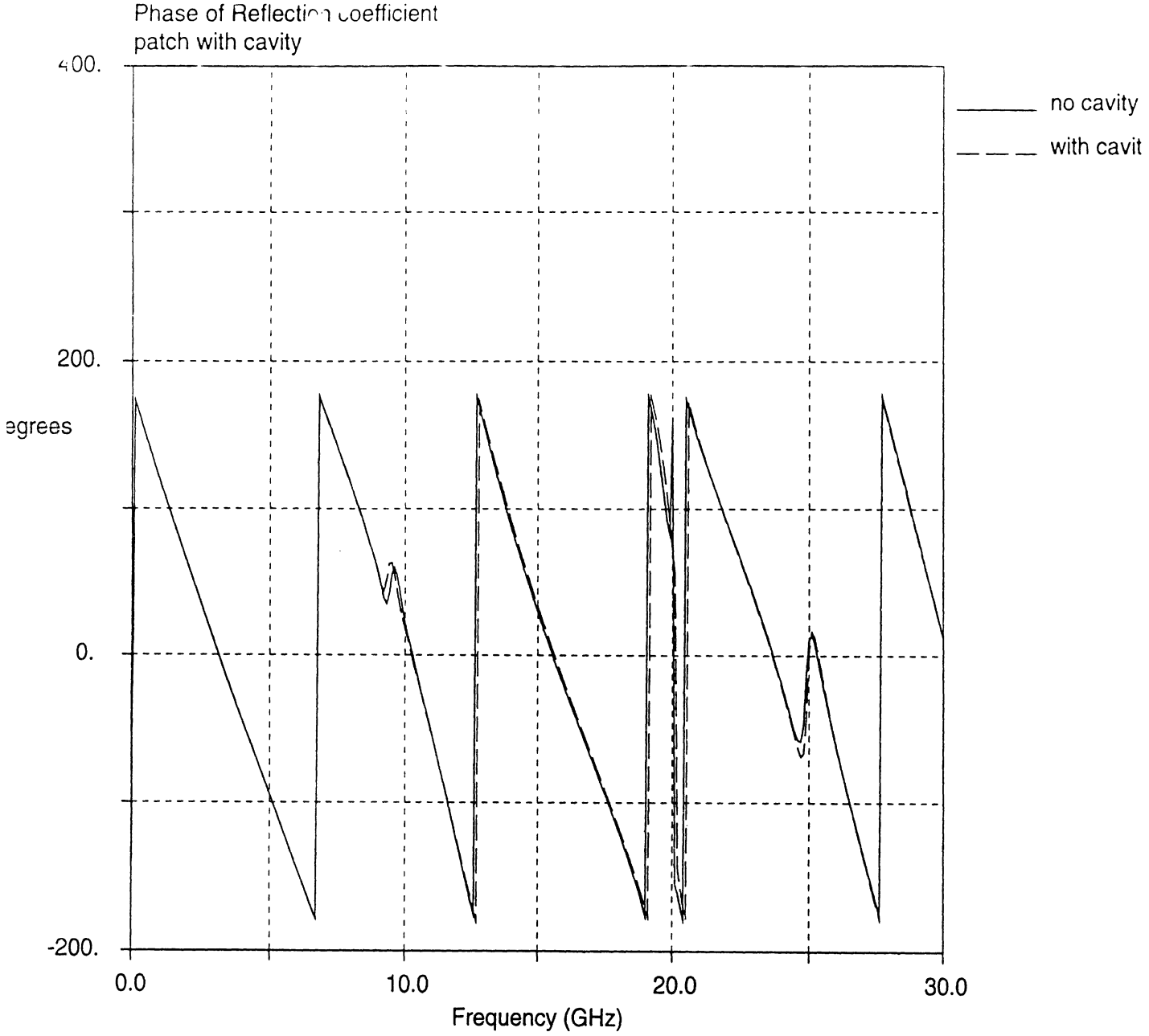

FIGURE 6. Comparison Between FDTD and IE for the Patch without the Cavity (Y_{os}=2.698mm).

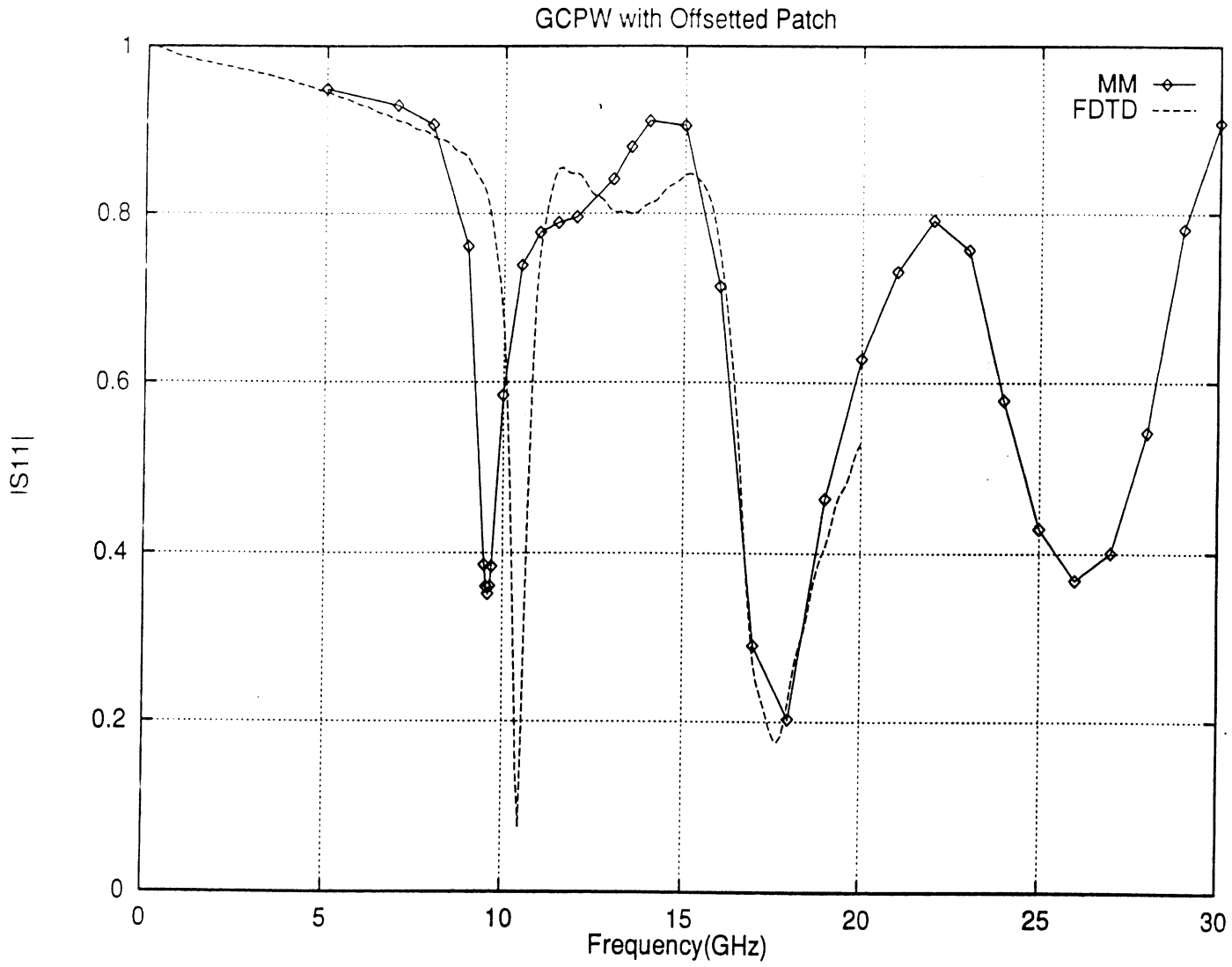

APPENDIX A: Finite Difference Time Domain Method

1 FDTD technique

The FDTD method was first introduced by Yee [2] to solve electromagnetic scattering problems. In this method, Maxwell's curl equations are expressed in discretized space and time domains and are then used to simulate the propagation of an initial excitation in a "leapfrog" manner. Recently, the method has been successfully applied to characterize microstrip and coplanar waveguide (CPW) lines and discontinuities [3]-[7], optical integrated circuits [8], and mm-wave and sub-mm-wave dielectric line transitions [1, 9]. Only a brief summary of the FDTD method is described here.

In order to characterize any planar structure, propagation of a specific time-dependent function through the structure is simulated using the FDTD technique. The time dependence of the excitation can be chosen arbitrarily; however, a Gaussian pulse is often used because it is smoothly varying in time and its Fourier transform is also a Gaussian function centered at zero frequency. Following the time and space discretizations of the electric and magnetic field components, the FDTD equivalents of Maxwell's equations are then used to update the spatial distributions of these components at alternating half time steps [10]. The space steps, Δx, Δy and Δz, are carefully chosen such that integral numbers of them can approximate the various dimensions of the structure. As a rule of thumb and in order to reduce the truncation and grid dispersion errors, the maximum step size is chosen to be less than 1/20 of the smallest wavelength existing in the computational domain (i.e., at the highest frequency represented in the pulse). Then, the Courant stability criterion is used to select the time step to insure numerical stability.

In order to excite the patch antenna, the vertical electric field component at the front plane (z=0) is excited and the magnetic wall source condition of [4] is used to compute the fields elsewhere in the plane z=0. For the electric field components lying on a dielectric-dielectric interface, the average between the two permittivities is used in the FDTD equations [3]. The super-absorbing first-order Mur boundary condition [11, 12] is utilized to terminate the FDTD lattice at the front (z=0) and back (z=N_z Δz, where N_z is the number of cells in the z-direction) planes in order to simulate infinite lines. This absorbing boundary condition requires a choice for the incident velocity of the waves, or equivalently ϵ_{eff}. It has been found that an appropriate choice of $\epsilon_{r,eff}$ minimizes the effect of the absorbing boundary walls. On the other hand, the first-order Mur boundary condition is used on the top and side walls to simulate an open structure. In general, the frequency dependent scattering parameters, S_{ij}, can be obtained as follows [3, 4]:

$$S_{ij}(\omega) = \frac{V_i(\omega)}{V_j(\omega)}\sqrt{\frac{Z_{0j}}{Z_{0i}}} \tag{1}$$

where V_i and V_j are the voltages at ports i and j, respectively, and Z_{0j} and Z_{0i} are the characteristic (or wave) impedances of the lines connected to these ports. To obtain $S_{11}(\omega)$, the incident and reflected fields must be known. Since the FDTD simulation calculates the total field (i.e., the sum of the incident and reflected waveforms), the incident field is obtained from that of an infinite extent line (i.e, from the source to far absorbing wall). Then, this incident field is subtracted from the total waveform to yield the reflected field.

References

[1] A. Engel, N. Dib and L. Katehi, "Characterization of a Shielded Transition to a Dielectric Waveguide," accepted for publication in the *IEEE Trans. MTT*.

[2] K. S. Yee, "Numerical solution of initial boundary value problems involving Maxwell's equations in isotropic media," *IEEE Trans. AP*, pp. 302-307, May 1966.

[3] X. Zhang and K. Mei, "Time-domain finite difference approach to the calculation of the frequency-dependent characteristics of microstrip discontinuities," *IEEE Trans. MTT*, pp. 1775–1787, Dec. 1988.

[4] D. Sheen, S. Ali, M. Abouzahra and J. Kong, "Application of the Three-Dimensional Finite-Difference Time-Domain Method to the Analysis of Planar Microstrip Circuits," *IEEE Trans. MTT*, pp. 849–857, July 1990.

[5] L. Wu and H. Chang, "Analysis of dispersion and series gap discontinuity in shielded suspended striplines with substrate mounting grooves," *IEEE Trans. MTT*, pp. 279–284, Feb. 1992.

[6] T. Shibata and H. Kimura, "Computer-Aided Engineering for Microwave and Millimeter-Wave Circuits Using the FD-TD Technique of Field Simulations," *It. J. of Microwave and Millimeter-Wave Computer-Aided Engineering*, Vol. 3, No. 3, pp. 238-250, 1993.

[7] S. Visan, O. Picon and V. Hanna, "3D Characterization of Air Bridges and Via Holes in Conductor-Backed Coplanar Waveguides for MMIC Applications," *1993 IEEE MTT-S Intl. Microwave Symp. Dig.*, pp. 709-712.

[8] S. Chu, W. Huang and S. Chaudhuri, "Simulation and Analysis of Waveguide Based Optical Integrated Circuits," *Computer Physics Communications*, vol. 68, pp. 451-484, 1991.

[9] N. Dib and L. Katehi, "Analysis of the Transition from Rectangular Waveguide to Shielded Dielectric Image Guide Using the Finite-Difference Time-Domain Method," *IEEE Microwave and Guided Wave Letters*, pp. 327-329, Sep. 1993.

[10] K. Kunz and R. Luebbers, *The Finite Difference Time Domain Method for Electromagnetics*, Florida: CRC press, 1993.

[11] G. Mur, "Absorbing boundary conditions for the finite-difference approximation of the time-domain electromagnetic-field equations," *IEEE Trans. EMC*, pp. 377–382, Nov. 1981.

[12] K. Mei and J. Fang, "Superabsorbtion-A method to improve absorbing boundary conditions," *IEEE Trans. AP*, pp. 1001–1010, Sep. 1992.

APPENDIX B: Finite Element/Integral Equation Method

Analysis of a Slot Coupled Coplanar Waveguide Fed Patch Antenna

Jui-Ching Cheng

November 29, 1993

1 Introduction

Fig. 1 shows a patch antenna that is fed by an open-ended coplanar waveguide(CPW) through a slot on the ground plane between the patch and the coplanar waveguide. A transverse slot on the CPW is used to increase the coupling efficiency. Full wave analysis and moment method are used in the analysis of this structure. Similar structures have been fully analyzed by the same method[1][3][4].

This analysis may be further extended to combine finite element method for more complex structures. As shown in Fig. 2, a patch is put on top of a cavity. If the shape of the cavity is complicated or the media inside the cavity is not simple, i.e., inhomogeneous or anisotropic, it is difficult to apply moment method in the cavity. Thus, the combination of finite element method and moment method is necessary to analyze this structure.

Section 2 will give a rigorous analysis of the problem. Section 3 includes the finite element method in the analysis of the cavity-backed patch antenna. Section 4 shows the preliminary numerical results. Details of finite element method formulation and Green's functions are given in appendix.

2 Theoretical Analysis

The schematic of the antenna and feed line is shown in Fig. 3. The ground plane and dielectric substrates extend to infinity in the x and y directions.

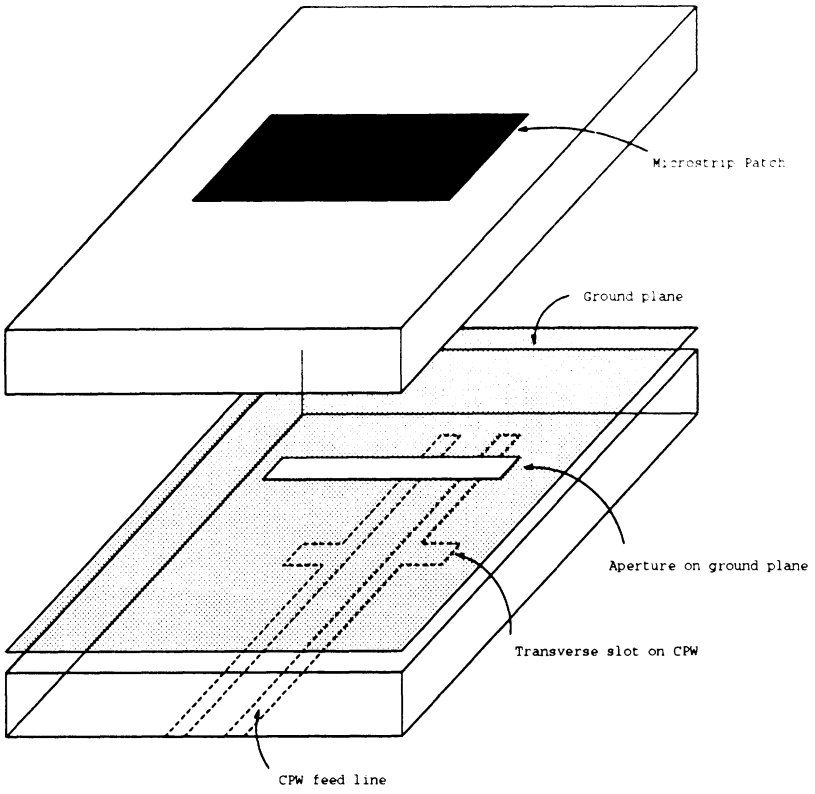

Figure 1: The structure of a slot coupled and CPW fed patch antenna.

By using equivalence principle, the original problem may be changed to an equivalent one which is shown in Fig 4. $\bar{J}_p$ denotes the induced current on the patch. The slot and the coplanar waveguide are closed by conductor such that the original structure is separated to 3 regions. In order to keep the same field distribution as the original one, magnetic surface currents $\bar{M}_{ap}$ must be added on the surface of the slot and also $\bar{M}_{inc}$ the equivalent incident traveling magnetic current mode on the CPW, and $\bar{M}_f$ the induced equivalent magnetic current on the CPW due to the field scattered by this structure. Furthermore, $\bar{M}_{ap}$ satisfy

$$\bar{M}_{ap} = \hat{z} \times \bar{E}_{ap}. \tag{1}$$

Let region a denote the lower dielectric slab, region b denote the upper dielectric slab and region c denote the free space below the CPW. The total

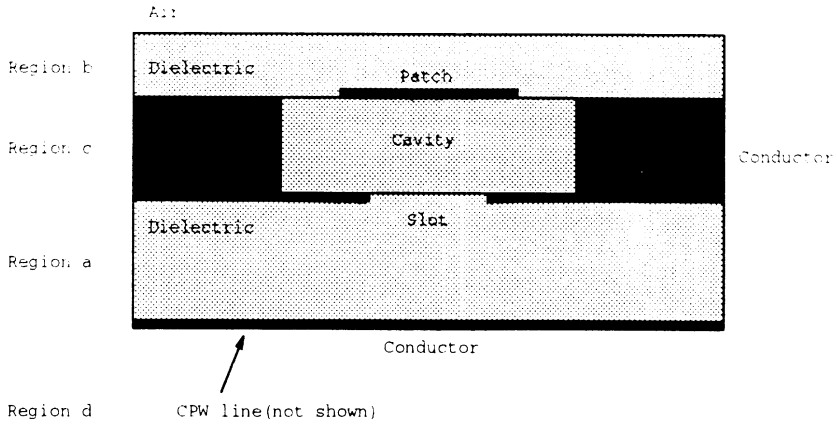

Figure 2: The structure of a slot coupled and cavity backed patch antenna.

electric and magnetic fields can be represented by superposition of fields due to the various currents as following equations:

$$\bar{E}_a^{tot} = \bar{E}_a(\bar{M}_{inc}) + \bar{E}_a(\bar{M}_f) + \bar{E}_a(\bar{M}_{ap}) \tag{2}$$

$$\bar{H}_a^{tot} = \bar{H}_a(\bar{M}_{inc}) + \bar{H}_a(\bar{M}_f) + \bar{H}_a(\bar{M}_{ap}) \tag{3}$$

$$\bar{E}_b^{tot} = \bar{E}_b(\bar{J}_p) - \bar{E}_b(\bar{M}_{ap}) \tag{4}$$

$$\bar{H}_b^{tot} = \bar{H}_b(\bar{J}_p) - \bar{H}_b(\bar{M}_{ap}) \tag{5}$$

$$\bar{E}_c^{tot} = -\bar{E}_c(\bar{M}_{inc}) - \bar{E}_c(\bar{M}_f) \tag{6}$$

$$\bar{H}_c^{tot} = -\bar{H}_c(\bar{M}_{inc}) - \bar{H}_c(\bar{M}_f). \tag{7}$$

Each field in equations (2)-(7) can be represented by dyadic Green's function for each structure such as

$$\bar{E}_b(\bar{M}_{ap}) = \iint_{slot} \bar{\bar{G}}_{EM}^b(x, y, z|x_0, y_0, z_0) \cdot \bar{M}_{ap}\, dx_0\, dy_0, \tag{8}$$

where $\bar{\bar{G}}_{EM}^b$ is the electric field at (x, y, z) due to an infinitesimal magnetic current at (x_0, y_0, z_0) radiating in the presence of a grounded dielectric slab. This and other Green's functions needed for the analysis are obtained by

using spectral domain methods so that

$$\overline{\overline{G}}^{b}_{EM}(x,y,z|x_0,y_0,z_0) = \int\int_{-\infty}^{\infty} \overline{\overline{Q}}^{b}_{EM}(k_x,k_y;z,z_0)\cdot e^{jk_x(x-x_0)}e^{jk_y(y-y_0)}\,dk_x\,dk_y. \tag{9}$$

Three coupled integral equations are obtained for the three unknown currents $\bar{M}_f$, $\bar{J}_p$, $\bar{M}_{ap}$ by enforcing the boundary conditions: 1) $\bar{H}^{tan}$ is continuous on the CPW, 2) $\bar{H}^{tan}$ is continuous through the slot, and 3) $\bar{E}^{tan}=0$ on the patch. That is,

$$\bar{E}_b(\bar{J}_p) - \bar{E}_b(\bar{M}_{ap}) = 0 \qquad \text{on the patch} \tag{10}$$

$$\bar{H}_a(\bar{M}_{inc}) + \bar{H}_a(\bar{M}_f) = -\bar{H}_c(\bar{M}_{inc}) - \bar{H}_c(\bar{M}_f) \qquad \text{on the CPW} \tag{11}$$

$$\bar{H}_a(\bar{M}_{inc}) + \bar{H}_a(\bar{M}_f) + \bar{H}_a(\bar{M}_{ap}) = \bar{H}_b(\bar{J}_p) - \bar{H}_b(\bar{M}_{ap}) \qquad \text{on the slot.} \tag{12}$$

Galerkin moment method is used to obtain the integral equations linking the unknown currents in region a and b.

The unknown currents are formulated by choosing expansion functions as follows:

$$\bar{J}_p(x,y) = \sum_{n=1}^{N_b} J_n^b \bar{J}_n^b(x,y) \tag{13}$$

$$\bar{M}_{ap}(x,y) = \sum_{n=1}^{N_{ap}} M_n^{ap} \bar{M}_n^{ap}(x,y) \tag{14}$$

$$\bar{M}_f(x,y) = \sum_{n=1}^{N_1} M_n^1 \bar{M}_n^1(x,y) + \sum_{n=1}^{N_2} M_n^2 \bar{M}_n^2(x,y) + R\bar{M}_{ref}(x,y), \tag{15}$$

where $\bar{M}_{ref}$ is the reflected traveling current mode on the CPW, $\bar{M}_n^1$ is the high order modes near the end of the CPW, $\bar{M}_n^2$ is the high order modes on the transverse slot on the CPW.

Define an inner product

$$(F,G)_s = \int\int_s \bar{F}\cdot\bar{G}\,ds. \tag{16}$$

The three boundary conditions lead to

$$\begin{gathered}[Z^b][I^b] + [T^b][M^{ap}] = 0 \\ [C^b][I^b] + ([Y^b]+[Y^a])[M^{ap}] + [Y^{ap,1}][M^1] + [Y^{ap,2}][M^2]\end{gathered} \tag{17}$$

$$+V_{inc}R([Y^{ap,c}] + j[Y^{ap,s}]) = -V_{inc}([Y^{ap,c}] - j[Y^{ap,s}]) \quad (18)$$

$$[Y^{1,1}][M^1] + [Y^{1,2}][M^2] + V_{inc}R([Y^{1,c}] + j[Y^{1,s}]) + [Y^{1,ap}][M^{ap}] = -V_{inc}([Y^{1,c}] - j[Y^{1,s}]) \quad (19)$$

$$[Y^{2,1}][M^1] + [Y^{2,2}][M^2] + V_{inc}R([Y^{2,c}] + j[Y^{2,s}]) + [Y^{2,ap}][M^{ap}] = -V_{inc}([Y^{2,c}] - j[Y^{2,s}]). \quad (20)$$

The last two equations come from the boundary condition 2. The matrix and vector elements are defined as follows:

$$y^a_{mn} = (-\bar{M}^{ap}_m, \bar{H}_a(\bar{M}^{ap}_n))_{ap} \quad N_{ap} \times N_{ap} \quad \text{matrix} \quad (21)$$

$$y^b_{mn} = (-\bar{M}^{ap}_m, \bar{H}_b(\bar{M}^{ap}_n))_{ap} \quad N_{ap} \times N_{ap} \quad \text{matrix} \quad (22)$$

$$y^{ap,1}_{mn} = (-\bar{M}^{ap}_m, \bar{H}_a(\bar{M}^1_n))_{ap} \quad N_{ap} \times N_1 \quad \text{matrix} \quad (23)$$

$$y^{ap,2}_{mn} = (-\bar{M}^{ap}_m, \bar{H}_a(\bar{M}^2_n))_{ap} \quad N_{ap} \times N_2 \quad \text{matrix} \quad (24)$$

$$y^{ap,c}_{mn} = (-\bar{M}^{ap}_m, \bar{H}_a(\bar{M}^c))_{ap} \quad N_{ap} \times 1 \quad \text{vector} \quad (25)$$

$$y^{ap,s}_{mn} = (-\bar{M}^{ap}_m, \bar{H}_a(\bar{M}^s))_{ap} \quad N_{ap} \times 1 \quad \text{vector} \quad (26)$$

$$y^{1,1}_{mn} = (-\bar{M}^1_m, (\bar{H}_a + \bar{H}_c)(\bar{M}^1_n))_f \quad N_1 + 1 \times N_1 \quad \text{matrix} \quad (27)$$

$$y^{1,2}_{mn} = (-\bar{M}^1_m, (\bar{H}_a + \bar{H}_c)(\bar{M}^2_n))_f \quad N_1 + 1 \times N_2 \quad \text{matrix} \quad (28)$$

$$y^{1,ap}_{mn} = (-\bar{M}^1_m, \bar{H}_a(\bar{M}^{ap}_n))_f \quad N_1 + 1 \times N_{ap} \quad \text{matrix} \quad (29)$$

$$y^{1,c}_{mn} = (-\bar{M}^1_m, (\bar{H}_a + \bar{H}_c)(\bar{M}^c_n))_f \quad N_1 + 1 \times 1 \quad \text{vector} \quad (30)$$

$$y^{1,s}_{mn} = (-\bar{M}^1_m, (\bar{H}_a + \bar{H}_c)(\bar{M}^s_n))_f \quad N_1 + 1 \times 1 \quad \text{vector} \quad (31)$$

$$y^{2,1}_{mn} = (-\bar{M}^2_m, (\bar{H}_a + \bar{H}_c)(\bar{M}^1_n))_f \quad N_2 \times N_1 \quad \text{matrix} \quad (32)$$

$$y^{2,2}_{mn} = (-\bar{M}^2_m, (\bar{H}_a + \bar{H}_c)(\bar{M}^2_n))_f \quad N_2 \times N_2 \quad \text{matrix} \quad (33)$$

$$y^{2,ap}_{mn} = (-\bar{M}^2_m, \bar{H}_a(\bar{M}^{ap}_n))_f \quad N_2 \times N_{ap} \quad \text{matrix} \quad (34)$$

$$y^{2,c}_{mn} = (-\bar{M}^2_m, (\bar{H}_a + \bar{H}_c)(\bar{M}^c_n))_f \quad N_2 \times 1 \quad \text{vector} \quad (35)$$

$$y^{2,s}_{mn} = (-\bar{M}^1_m, (\bar{H}_a + \bar{H}_c)(\bar{M}^s_n))_f \quad N_2 \times 1 \quad \text{vector} \quad (36)$$

$$z^b_{mn} = (-\bar{J}^b_m, \bar{E}_b(\bar{J}^b_n))_p \quad N_b \times N_b \quad \text{matrix} \quad (37)$$

$$t^b_{mn} = (\bar{J}^b_m, \bar{E}_b(\bar{M}^{ap}_n))_p \quad N_{ap} \times N_{ap} \quad \text{matrix} \quad (38)$$

$$c^b_{mn} = (\bar{M}^{ap}_m, \bar{H}_b(\bar{J}^b_n))_{ap} \quad N_{ap} \times N_b \quad \text{matrix} \quad (39)$$

$$I^b_n = J^b_1, J^b_2, \cdots, J^b_{N_b} \quad N_b \times 1 \quad \text{column vector} \quad (40)$$

$$M^1_n = M^1_1, M^1_2, \cdots, M^1_{N_1} \quad N_1 \times 1 \quad \text{column vector} \quad (41)$$

$$M^2_n = M^2_1, M^2_2, \cdots, M^2_{N_2} \quad N_2 \times 1 \quad \text{column vector} \quad (42)$$

$$M^{ap}_n = M^{ap}_1, M^{ap}_2, \cdots, M^{ap}_{N_{ap}} \quad N_{ap} \times 1 \quad \text{column vector} \quad (43)$$

(44)

Note that on the CPW extra higher order current mode is used as a test function to avoid using traveling current mode such that computation complexity is reduced. From reciprocity, the following relations exist.

$$y_{mn}^{ap,1} = y_{nm}^{1,ap} \tag{45}$$

$$y_{mn}^{2,1} = y_{nm}^{1,2}. \tag{46}$$

Recast some of the quantities above into new forms:

$$[M^{tot}] = \begin{bmatrix} M^1 \\ M^2 \\ V_{inc}R \end{bmatrix} \tag{47}$$

$$[Y^{12}] = \begin{bmatrix} Y^{1,1} & Y^{1,2} \\ Y^{2,1} & Y^{2,2} \end{bmatrix} \tag{48}$$

$$[Y^{12,c}] = \begin{bmatrix} Y^{1,c} \\ Y^{2,c} \end{bmatrix} \tag{49}$$

$$[Y^{12,s}] = \begin{bmatrix} Y^{1,s} \\ Y^{2,s} \end{bmatrix} \tag{50}$$

$$[Y^{12,ap}] = \begin{bmatrix} Y^{1,ap} \\ Y^{2,ap} \end{bmatrix} \tag{51}$$

$$[Y^{tot}] = [Y^{12}|Y^{12,c} + jY^{12,s}] \tag{52}$$

$$[Y^{ap,12}] = [Y^{ap,1}|Y^{ap,2}] \tag{53}$$

$$[Y^{ap}] = \left[Y^a + Y^b\right] \tag{54}$$

$$[Y^{ap,tot}] = [Y^{ap,12}|Y^{ap,c} + jY^{ap,s}] \tag{55}$$

$$[V^{inc}] = -V_{inc}([Y^{12,c}] - j[Y^{12,s}]) \tag{56}$$

$$[M^{inc}] = -V_{inc}([Y^{ap,c}] - j[Y^{ap,s}]). \tag{57}$$

Substituting the above equations to (17)–(20) and rearranging yield

$$[Y^{12,tot}][M^{tot}] + [Y^{12,ap}][M^{ap}] = [V^{inc}] \tag{58}$$

$$[Z^b][I^b] + [T^b][M^{ap}] = 0 \tag{59}$$

$$[C^b][I^b] + [Y^{ap}][M^{ap}] + [Y^{ap,tot}][M^{tot}] = [M^{inc}]. \tag{60}$$

Solving (58)-(60) simultaneously, we get

$$[I^b] = -[Z^b]^{-1}[T^b][M^{ap}] \quad (61)$$

$$[M^{tot}] = [Y^{12,tot}]^{-1}([V^{inc}] - [Y^{12,ap}][M^{ap}]) \quad (62)$$

$$[M^{ap}] = ([Y^{ap}] - [C^b][Z^b]^{-1}[T^b] - [Y^{ap,tot}][Y^{12,tot}]^{-1}[Y^{12,ap}])^{-1} ([M^{inc}] - [Y^{ap,tot}][Y^{12,tot}]^{-1}[V^{inc}]). \quad (63)$$

Such the unknown quantities $[M^{ap}]$, $[M^{tot}]$ and $[I^b]$ are solved in terms of matrix equations (61)-(63).

Assume the CPW is very narrow such that only y-directed magnetic currents exist, i.e. $\bar{M}_{inc}$, $\bar{M}_{ref}$ and $\bar{M}_1$ only have y component. Also assume the slots on ground plane and CPW are small such that only x directed magnetic currents exist. the current modes on patch are the same as that in [1] and are not shown here. The incident and reflected currents are represented by traveling current mode which is the fundamental CPW mode. The traveling current mode is further separated to sine and cosine part as follows

$$\bar{M}_{inc}(x,y) = \hat{y}(M^c(x,y) - jM^s(x,y)) \quad (64)$$

$$\bar{M}_{ref}(x,y) = \hat{y}R(M^c(x,y) + jM^s(x,y)), \quad (65)$$

where

$$M^c(x,y) = \begin{cases} f_x(x)\cos k_{ea}(y-L), & \text{for } -m\lambda_e - \frac{\lambda_e}{4} \le y - L \le -\frac{\lambda_e}{4} \\ 0, & \text{elsewhere} \end{cases} \quad (66)$$

$$M^s(x,y) = \begin{cases} f_x(x)\sin k_{ea}(y-L), & \text{for } -m\lambda_e \le y - L \le 0 \\ 0, & \text{elsewhere} \end{cases} \quad (67)$$

$$f_x(x) = \begin{cases} \frac{1}{W_f}, & \text{for } \frac{S}{2} \le x \le \frac{S}{2} + W_f \\ \frac{-1}{W_f}, & \text{for } -\frac{S}{2} \ge x \ge \frac{S}{2} - W_f \\ 0, & \text{elsewhere.} \end{cases} \quad (68)$$

k_{ea} is the propagation constant of the fundamental mode of CPW. It is derived by the method of [5]. λ_e is the equivalent wavelength. m is a parameter to be chosen. The Fourier transforms of M^c and M^s are

$$\tilde{M}^c = \tilde{f}_x k_{ea} e^{jk_y(\frac{\lambda_e}{4} - L)} \frac{e^{jk_y m\lambda_e} - 1}{k_e^2 - k_y^2} \quad (69)$$

and

$$\tilde{M}^s = \tilde{f}_x k_{ea} e^{-jk_y L} \frac{e^{jk_y n_i \lambda_e} - 1}{k_\epsilon^2 - k_y^2}. \tag{70}$$

where $\tilde{f}_x$ is the fourier transform of f_x and

$$\tilde{f}_x(k_x) = \frac{2j}{W_f} \frac{\cos k_x(\frac{S}{2} + W_f) - \cos k_x \frac{S}{2}}{k_x}. \tag{71}$$

Most of the basis functions are represented by piecewise sinusoidal(PWS) modes(see Fig 5) as follows.

For $\bar{M}_n^1$ not on the boundary of the slot,

$$\bar{M}_n^1 = \begin{cases} \hat{x} f_x(x) \frac{\sin k(h - |y - y_n|)}{\sin kh}, & \text{for} \quad |y - y_n| \le h \\ 0, & \text{elsewhere} \end{cases}, \tag{72}$$

and k is chosen to be $(k_{ea} + k_0)/2$, h is half of the width of the PWS mode. The fourier transform of $\bar{M}_n^1$ is

$$\tilde{M}_n^1(k_x, k_y) = \tilde{f}_x(k_x) \frac{2ke^{-jk_y y_n}}{\sin kh} \frac{\cos k_y h - \cos kh}{k^2 - k_y^2}. \tag{73}$$

For $\bar{M}_n^1$ on the boundary of the slot,

$$\bar{M}_n^1 = \begin{cases} \hat{y} f_x(x) \frac{\sin k(h_1 - |y - y_n|)}{\sin kh_1}, & \text{for} \quad y_n - h_1 \le y \le y_n \\ \hat{y} f_x(x) \frac{\sin k(h_2 - |y - y_n|)}{\sin kh_2}, & \text{for} \quad y_n \le y \le y_n + h_2 \\ 0, & \text{elsewhere} \end{cases} \tag{74}$$

and

$$\begin{aligned} \tilde{M}_n^1(k_x, k_y) \;=\; & \tilde{f}_x(k_x) e^{-jk_y y_n} \left[\frac{ke^{jk_y h_1} - k \cos kh_1 - jk_y \sin kh_1}{\sin kh_1 (k^2 - k_y^2)} \right. \\ & \left. + \frac{ke^{-jk_y h_2} - k \cos kh_2 + jk_y \sin kh_2}{\sin kh_2 (k^2 - k_y^2)} \right]. \end{aligned} \tag{75}$$

For $\bar{M}_n^2$ not on the boundary of the CPW,

$$\bar{M}_n^2 = \begin{cases} \hat{x} f_y(y) \frac{\sin k(h - |x - x_n|)}{\sin kh}, & \text{for} \quad |x \pm x_n| \le h \\ 0, & \text{elsewhere} \end{cases}, \tag{76}$$

where

$$f_y(y) = \begin{cases} \frac{1}{W_2}, & \text{for } -\frac{W_2}{2} \le y \le \frac{W_2}{2} \\ 0, & \text{elsewhere.} \end{cases} \quad (77)$$

k is chosen to be $(k_{ea} + k_0)/2$ and

$$\tilde{M}_n^2(k_x, k_y) = \tilde{f}_y(k_y) 2 \cos k_x x_n \frac{2k}{\sin kh} \frac{\cos k_x h - \cos kh}{k^2 - k_x^2}, \quad (78)$$

where $\tilde{f}_y$ is the fourier transform of f_y and

$$\tilde{f}_y(k_y) = \frac{\sin k_y \frac{W_2}{2}}{k_y \frac{W_2}{2}}. \quad (79)$$

For $\bar{M}_n^2$ on the boundary of the CPW,

$$\begin{aligned} \tilde{M}_n^2(k_x, k_y) &= \tilde{f}_y(k_y) \left[\frac{2k \cos(k_x h_1 - k_x x_n) - 2k \cos kh_1 \cos k_x x_n - 2k_x \sin kh_1 \sin k_x x_n}{\sin kh_1 (k^2 - k_x^2)} \right. \\ &\left. + \frac{2k \cos(k_x h_2 + k_x x_n) - 2k \cos kh_2 \cos k_x x_n + 2k_x \sin kh_2 \sin k_x x_n}{\sin kh_2 (k^2 - k_x^2)} \right]. \quad (80) \end{aligned}$$

For $\bar{M}_{ap}$

$$\bar{M}_n^{ap} = \hat{x} f_y(y) \frac{\sin k(h - |x - x_n|)}{\sin kh} \quad (81)$$

k is chosen as that of [1], and

$$\tilde{M}_n^{ap} = \tilde{f}_y(k_y) \frac{2ke^{-jk_x x_n}}{\sin kh} \frac{\cos k_x h - \cos kh}{k^2 - k_x^2}. \quad (82)$$

Since there are poles in the Green's functions. Pole extraction method [3] is used. The integrand always takes the form

$$I = \int_0^{2\pi} \int_0^{\infty} \frac{f(\beta, \phi)}{k_z \sin k_z d} \beta d\beta d\phi, \quad (83)$$

where $k_z = \sqrt{k^2 - \beta^2}$. Rewrite I as

$$\begin{aligned} I &= \int_0^{2\pi} \int_0^{\infty} \left[\frac{f(\beta, \phi)}{k_z \sin k_z d} - \frac{G^r f(k, \phi) 2k^2/\beta}{\beta^2 - k^2} \right] \beta d\beta d\phi \\ &+ \int_0^{2\pi} \int_0^{\infty} \frac{G^r f(k, \phi) 2k^2}{\beta^2 - k^2} d\beta d\phi, \quad (84) \end{aligned}$$

where G^r is the residue of $1/(k_z \sin k_z d)$ at $\beta = k$ which is equal to $-1/2kd$.
The third term of I can be evaluated analytically, which is equal to $\int_0^{2\pi} f(k, \phi) G^r (-j\pi k) d\phi$.

3 Combination of Finite Element Method and Moment method

The schematic of the cavity-backed patch antenna and feed line is shown in Fig. 6 with impressed and induced currents indicated. Following the same notation and procedure as the previous section, the boundary conditions can be expressed as

$$\bar{H}_a(\bar{M}_{inc}) + \bar{H}_a(\bar{M}_f) + \bar{H}_a(\bar{M}_{ap}) = -\bar{H}_d(\bar{M}_{inc}) - \bar{H}_d(\bar{M}_f) \quad \text{on the CPW} \tag{85}$$

$$\bar{H}_a(\bar{M}_{inc}) + \bar{H}_a(\bar{M}_f) + \bar{H}_a(\bar{M}_{ap}) = \bar{H}_c(\bar{M}_p) - \bar{H}_c(\bar{M}_{ap}) \quad \text{on the slot} \tag{86}$$

$$-\bar{H}_b(\bar{M}_p) = \bar{H}_c(\bar{M}_p) - \bar{H}_c(\bar{M}_{ap}) \quad \text{on cavity opening,} \tag{87}$$

where subscripts a,b,c and d denote the regions shown in Fig 2, and $\bar{M}_{inc}$, $\bar{M}_f$, $\bar{M}_{ap}$ and $\bar{M}_p$ are the equivalent sources shown in Fig 7. The fields in the cavity are obtained by using finite element method, which is shown in appendix. Greens function technique is used to obtain the fields in other regions.

Since the structures of Fig 1 and Fig 2 only differ in the cavity and patch parts, only small modification is necessary to the formulations in previous section. Thus, the following matrix equation is obtain.

$$[Y^b][M^p] = -[Y^p][M^p] + [Y^{p,ap}][M^{ap}] \tag{88}$$

$$\begin{aligned}[Y^{ap}][M^{ap}] + [Y^a][M^{ap}] - [Y^{ap,p}][M^p] + [Y^{ap,1}][M^1] + [Y^{ap,2}][M^2] \\ +V_{inc}R([Y^{ap,c}] + j[Y^{ap,s}]) = -V_{inc}([Y^{ap,c}] - j[Y^{ap,s}])\end{aligned} \tag{89}$$

$$\begin{aligned}[Y^{1,1}][M^1] + [Y^{1,2}][M^2] + V_{inc}R([Y^{1,c}] + j[Y^{1,s}]) \\ +[Y^{1,ap}][M^{ap}] = -V_{inc}([Y^{1,c}] - j[Y^{1,s}])\end{aligned} \tag{90}$$

$$\begin{aligned}[Y^{2,1}][M^1] + [Y^{2,2}][M^2] + V_{inc}R([Y^{2,c}] + j[Y^{2,s}]) \\ +[Y^{2,ap}][M^{ap}] = -V_{inc}([Y^{2.c}] - j[Y^{2,s}]).\end{aligned} \tag{91}$$

The definition of the matrices and vectors which are different from previous section are shown as follows:

$$y^b_{mn} = (-\bar{M}^p_m, \bar{H}_b(\bar{M}^p_n))_p \quad N_p \times N_p \quad \text{matrix} \tag{92}$$

$$y^p_{mn} = (-\bar{M}^p_m, \bar{H}_c(\bar{M}^p_n))_p \quad N_p \times N_p \quad \text{matrix} \tag{93}$$

$$y^{ap}_{mn} = (-\bar{M}^{ap}_m, \bar{H}_c(\bar{M}^{ap}_n))_{ap} \quad N_{ap} \times N_{ap} \quad \text{matrix} \tag{94}$$

$$y_{mn}^{ap,p} = (-\bar{M}_m^{ap}, \bar{H}_c(\bar{M}_n^p))_{ap} \quad N_{ap} \times N_p \quad \text{matrix} \tag{95}$$

$$y_{mn}^{p,ap} = (-\bar{M}_m^{p}, \bar{H}_c(\bar{M}_n^{ap}))_{p} \quad N_{p} \times N_{ap} \quad \text{matrix}. \tag{96}$$

Equations (93)-(96) are calculated by finite element method which is shown in appendix.

Recast some of the quantities above into new forms:

$$[Y_{tot}^b] = [y^b + y^p] \quad N_p \times N_p \quad \text{matrix} \tag{97}$$

$$[Y_{tot}^a] = [y^a + y^{ap}] \quad N_{ap} \times N_{ap} \quad \text{matrix}. \tag{98}$$

Substituting the above equations to (88)-(91) and rearranging yield

$$[Y_{tot}^b][M^p] = [Y^{ps}][M^s] \tag{99}$$

$$[Y^{12,tot}][M^{tot}] + [Y^{12,ap}][M^{ap}] = [V^{inc}] \tag{100}$$

$$[Y_{tot}^a][M^{ap}] - [Y^{ap,p}][M^{ap}] + [Y^{ap,tot}][M^{tot}] = [M^{inc}]. \tag{101}$$

Solving (99)-(101) simultaneously, we get

$$[M^p] = [Y_{tot}^b]^{-1}[Y^{ps}][M^s] \tag{102}$$

$$[M^{tot}] = [Y^{12,tot}]^{-1}([V^{inc}] - [Y^{12,ap}][M^{ap}]) \tag{103}$$

$$[M^{ap}] = ([Y_{tot}^a] - [Y^{ap,p}][Y_{tot}^b]^{-1}[Y^{p,ap}] - [Y^{ap,tot}][Y^{12,tot}]^{-1}[Y^{12,ap}])^{-1} ([M^{inc}] - [Y^{ap,tot}][Y^{12,tot}]^{-1}[V^{inc}]). \tag{104}$$

Such the unknown quantities are solved.

4 Numerical Results

Since the CPW line is very narrow, only y-directed magnetic currents are used to model the currents on it. Also assume the aperture on the ground plane and the transverse slot on the CPW are narrow enough that only x-directed magnetic currents are necessary to model the currents on them. The currents on the patch are assumed to be only y-directed too. The incident and reflected currents are represented by traveling wave modes which are the fundamental CPW modes. It is further separated to sine and cosine parts as in [1]. Since infinite traveling wave modes produce extra poles in spectral domain, it is truncated at sufficient large distance from the end of the CPW.

The cosine part of the traveling wave mode is ended at a quarter wavelength from the end of the CPW to avoid a not zero current at the end of CPW. The propagation constant of the fundamental mode of CPW is calculated by the method of [5]. Although there is a small imaginary part in the propagation constant, it is not taken into account because it is much smaller than the real part. Typically, the ratio is smaller than 1/100. The dimension of the structure is the same as [6] as shown in Fig. 3. All the basis functions used are piecewise sinusoidal(PWS) modes.

Fig. 8 shows the variation of the amplitude of S_{11} v.s. the number of basis functions used on CPW. Good convergence is reached with 7 basis functions. Fig. 9 shows the amplitude of S_{11} v.s. frequency.

After the correctness of the analysis of section 2 is confirmed by comparison of the numerical results with other methods, the finite element method part will be included in the programs to analyze the cavity-backed patch antenna.

Appendix

A Finite Element Formulations

In the cavity, the magnetic field satisfies

$$\nabla \times (-\frac{1}{j\omega\epsilon_c}\nabla \times \bar{H}_c) = j\omega\mu_c\bar{H}_c. \tag{105}$$

Let $\bar{\phi}_i$ denotes the test functions. Integrating the test functions with equation (105) in the whole volume of the cavity leads to

$$\iiint_{V_c}[\nabla \times (-\frac{1}{j\omega\epsilon_c}\nabla \times \bar{H}_c)] \cdot \bar{\phi}_i \, dv - \iiint_{V_c}(j\omega\mu_c\bar{H}_c \cdot \bar{\phi}_i) \, dv = 0. \tag{106}$$

Integration by parts the first term in (106), we obtain:

$$\begin{aligned}\iiint_{V_c}(-\frac{1}{j\omega\epsilon_c}\nabla \times \bar{H}_c) \cdot \nabla \times \bar{\phi}_i \, dv - \iiint_{V_c}(j\omega\mu_c\bar{H}_c \cdot \bar{\phi}_i) \, dv \\ = \iint_S (\hat{n} \times \bar{E}_c) \cdot \bar{\phi}_i \, ds = -\iint_S \bar{M}_c \cdot \bar{\phi}_i \, ds,\end{aligned} \tag{107}$$

where S is the surface of the cavity. Because the cavity is surrounded by conductor except the slot and the opening around the patch, $\bar{M}_c$ is $\bar{M}_p$ or $-\bar{M}_{ap}$. Let $\bar{H}_c$ represented by basis functions $\bar{\Phi}_i$

$$\bar{H}_c = \sum_{i=1}^{N_\Phi} \Phi_i\bar{\Phi}_i. \tag{108}$$

Then the following equations is obtained

$$\bar{H}_c(\bar{M}_{ap}) = [\bar{\Phi}][S][M^{ap}] \tag{109}$$

$$\bar{H}_c(\bar{M}_p) = [\bar{\Phi}][P][M^p]. \tag{110}$$

Where $[\bar{\Phi}] = [\bar{\Phi}_1\bar{\Phi}_2\bar{\Phi}_3\cdots]$ is a row vector, $[P]$ and $[S]$ are $N_\Phi \times N_p$ and $N_\Phi \times N_s$ matrices respectively. Column j of $[S]$ and $[P]$ are the finite element solutions

of equation (107) due to $\bar{M}_j^s$ and M_j^p respectively. Now we can express $[Y^s]$, $[Y^p]$, $[Y^{sp}]$ and $[Y^{ps}]$ as follows:

$$[Y^s] = [\Phi^s][S] \tag{111}$$
$$[Y^p] = [\Phi^p][P] \tag{112}$$
$$[Y^{sp}] = [\Phi^s][P] \tag{113}$$
$$[Y^{ps}] = [\Phi^p][S]. \tag{114}$$

where

$$\Phi^s_{mn} = (-\bar{M}^s_m, \bar{\Phi}_n)_s \quad N_s \times N_\Phi \quad \text{matrix} \tag{115}$$
$$\Phi^p_{mn} = (-\bar{M}^p_m, \bar{\Phi}_n)_p \quad N_p \times N_\Phi \quad \text{matrix.} \tag{116}$$

B Green's Functions

The spectral domain kernels that are used for the Green's functions of the analysis are presented below. The following definitions are used in the expressions:

$$k_0^2 = \omega^2 \mu_0 \epsilon_0 \tag{117}$$
$$k_{1a} = (\epsilon_r^a k_0^2 - \beta^2)^{1/2}, \qquad Im\{k_{1a}\} < 0, Re\{k_{1a}\} > 0 \tag{118}$$
$$k_{1b} = (\epsilon_r^b k_0^2 - \beta^2)^{1/2}, \qquad Im\{k_{1b}\} < 0, Re\{k_{1b}\} > 0 \tag{119}$$
$$k_2 = (k_0^2 - \beta^2)^{1/2}, \qquad Im\{k_2\} < 0, Re\{k_2\} > 0 \tag{120}$$
$$\beta^2 = k_x^2 + k_y^2 \tag{121}$$
$$T_e^b = k_{1b}\cos(k_{1b}d_b) + jk_2\sin(k_{1b}d_b) \tag{122}$$
$$T_m^b = \epsilon_r^b k_2\cos(k_{1b}d_b) + jk_{1b}\sin(k_{1b}d_b) \tag{123}$$
$$Z_0 = (\mu_0/\epsilon_0)^{1/2} \tag{124}$$

The required kernel functions are listed below.

For $G^b_{EJyy}(x, y, d_b|x_0, y_0, d_b)$:

$$\begin{aligned} Q^b_{EJyy}(k_x, k_y) \;=\; & -j\frac{Z_0}{4\pi^2 k_0} \\ & \cdot\frac{(\epsilon_r^b k_0^2 - k_y^2)k_2\cos(k_{1b}d_b) + j(k_0^2 - k_y^2)k_{1b}\sin(k_{1b}d_b)}{T_e^b T_m^b} \\ & \times \sin(k_{1b}d_b) \end{aligned} \tag{125}$$

For $G^b_{HJxy}(x,y,0|x_0,y_0,d_b)$:

$$Q^b_{HJxy}(k_x,k_y)=\frac{1}{4\pi^2}\cdot\frac{-\epsilon^b_r k_{1b}k_2\cos(k_{1b}d_b)+j(k_y^2(\epsilon^b_r-1)-k^2_{1b})\sin(k_{1b}d_b)}{T^b_e T^b_m} \tag{126}$$

For $G^b_{HMxx}(x,y,0|x_0,y_0,0)$:

$$\begin{aligned}Q^b_{HMxx}(k_x,k_y) &= \frac{-j}{4\pi^2 k_0 Z_0}\frac{1}{k_{1b}T^b_e T^b_m}\cdot[jk_x^2k_{1b}^2(\epsilon^b_r-1)+(\epsilon^b_r k_0^2-k_x^2)\\ &\quad\times\{k_{1b}k_2(\epsilon^b_r+1)\sin(k_{1b}d_b)\cos(k_{1b}d_b)\\ &\quad+j(\epsilon^b_r k_2^2\sin^2(k_{1b}d_b)-k^2_{1b}\cos^2(k_{1b}d_b))\}]\end{aligned} \tag{127}$$

For $G^b_{EMyx}(x,y,d_b|x_0,y_0,0)$

$$Q^b_{EMyx}(k_x,k_y)(k_x,k_y)=-Q^b_{HJxy}(k_x,k_y) \tag{128}$$

For $G^a_{HMxx}(x,y,0|x_0,y_0,0)$:

$$Q^a_{HMxx}(k_x,k_y)=\frac{j\omega\epsilon_0}{4\pi^2k_0^2}\cdot(\epsilon^a_r k_0^2-k_x^2)\cdot\frac{\cos(k_{1a}d_a)}{k_{1a}\sin(k_{1a}d_a)} \tag{129}$$

For $G^a_{HMyy}(x,y,0|x_0,y_0,0)$:

$$Q^a_{HMyy}(k_x,k_y)=\frac{j\omega\epsilon_0}{4\pi^2k_0^2}\cdot(\epsilon^a_r k_0^2-k_y^2)\cdot\frac{\cos(k_{1a}d_a)}{k_{1a}\sin(k_{1a}d_a)} \tag{130}$$

For $G^a_{HMxx}(x,y,d|x_0,y_0,0)$:

$$Q^a_{HMxx}(k_x,k_y)=\frac{j\omega\epsilon_0}{4\pi^2k_0^2}\cdot(\epsilon^a_r k_0^2-k_x^2)\cdot\frac{1}{k_{1a}\sin(k_{1a}d_a)} \tag{131}$$

For $G^a_{HMxy}(x,y,0|x_0,y_0,0)$:

$$Q^a_{HMxy}(k_x,k_y)=\frac{-j\omega\epsilon_0}{4\pi^2k_0^2}\cdot(k_xk_y)\cdot\frac{\cos(k_{1a}d_a)}{k_{1a}\sin(k_{1a}d_a)} \tag{132}$$

For $G^a_{HMyx}(x,y,0|x_0,y_0,d)$:

$$Q^a_{HMyx}(k_x,k_y)=\frac{-j\omega\epsilon_0}{4\pi^2k_0^2}\cdot(k_xk_y)\cdot\frac{1}{k_{1a}\sin(k_{1a}d_a)} \tag{133}$$

For $G^c_{HMxy}(x,y,0|x_0,y_0,0)$:

$$Q^c_{HMyx}(k_x,k_y) = \frac{\omega\epsilon_0}{4\pi^2 k_0^2}\cdot(k_x k_y)\cdot\frac{1}{k_2} \tag{134}$$

For $G^c_{HMxx}(x,y,0|x_0,y_0,0)$:

$$Q^c_{HMxx}(k_x,k_y) = \frac{-\omega\epsilon_0}{4\pi^2 k_0^2}\cdot(k_0^2-k_x^2)\cdot\frac{1}{k_2} \tag{135}$$

For $G^c_{HMyy}(x,y,0|x_0,y_0,0)$:

$$Q^c_{HMyy}(k_x,k_y) = \frac{-\omega\epsilon_0}{4\pi^2 k_0^2}\cdot(k_0^2-k_y^2)\cdot\frac{1}{k_2} \tag{136}$$

Because of reciprocity and symmetry, the following equations also hold.

$$G^a_{HMxx}(x,y,d|x_0,y_0,d) = G^a_{HMxx}(x,y,0|x_0,y_0,0) \tag{137}$$
$$G^a_{HMyy}(x,y,d|x_0,y_0,d) = G^a_{HMyy}(x,y,0|x_0,y_0,0) \tag{138}$$
$$G^a_{HMxx}(x,y,d|x_0,y_0,0) = G^a_{HMxx}(x,y,0|x_0,y_0,d) \tag{139}$$
$$G^a_{HMxy}(x,y,d|x_0,y_0,0) = G^a_{HMyx}(x,y,0|x_0,y_0,d) \tag{140}$$
$$G^a_{HMxy}(x,y,0|x_0,y_0,0) = G^a_{HMyx}(x,y,0|x_0,y_0,0) \tag{141}$$
$$G^c_{HMxy}(x,y,0|x_0,y_0,0) = G^c_{HMyx}(x,y,0|x_0,y_0,0) \tag{142}$$

References

[1] P.L. Sullivan and D.H. Schaubert, "Analysis of an Aperture Coupled Microstrip Antenna," *IEEE Trans. Antennas Propagat.,* vol. AP-34, pp. 977–984, Aug. 1986.

[2] D. M. Pozar, "Input impedance and mutual coupling of rectangular microstrip antennas," *IEEE Trans. Antennas Propagat.,* vol. AP-30, pp. 1191-1196, Nov. 1982.

[3] N.K. Das and D.M. Pozar, "Multiport Scattering Analysis of General Multilayered Printed Antennas Fed by Multiple Feed Ports: Part I — Theory," *IEEE Trans. Antennas Progagat.,* vol. AP-40, pp. 469–481, May 1992.

[4] N.K. Das and D.M. Pozar, "Multiport Scattering Analysis of General Multilayered Printed Antennas Fed by Multiple Feed Ports: Part II — Applications," *IEEE Trans. Antennas Progagat.*, vol. AP-40, pp. 482-490, May 1992.

[5] R.W. Jackson and D.M. Pozar, "Full-wave analysis of microstrip open-end and gap discontinuities," *IEEE Trans. Microwave Theory Tech.*, vol. MTT-33, pp. 1036-1042, Oct. 1985.

[6] R.N. Simons and R.Q. Lee, "Coplanar waveguide aperture coupled patch antennas with ground plane/substrate of finite extent."

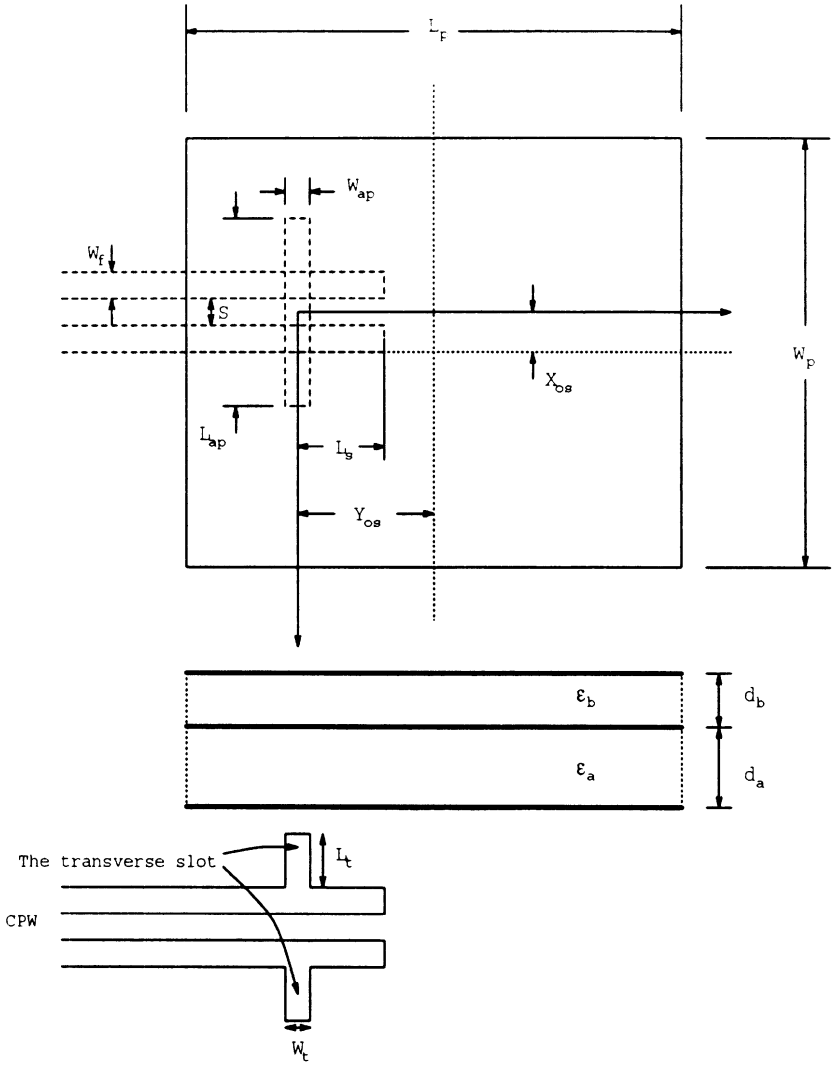

Figure 3: The schematic of the original problem.

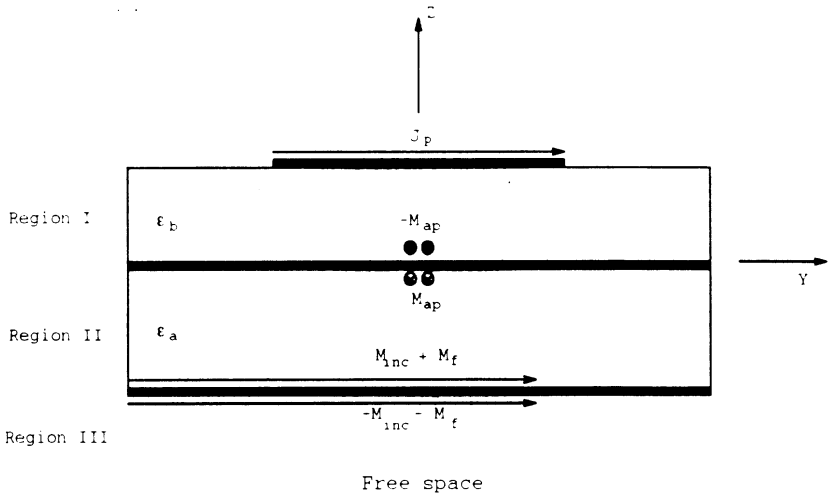

Figure 4: The equivalent problem after closing the slot by conductor. Suitable magnetic currents are added to ensure the equivalence.

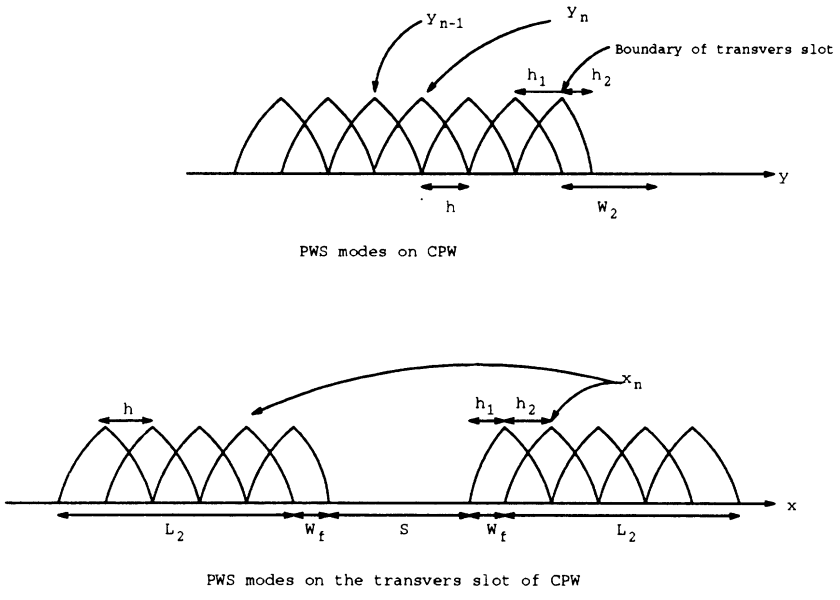

Figure 5: The PWS modes on the CPW.

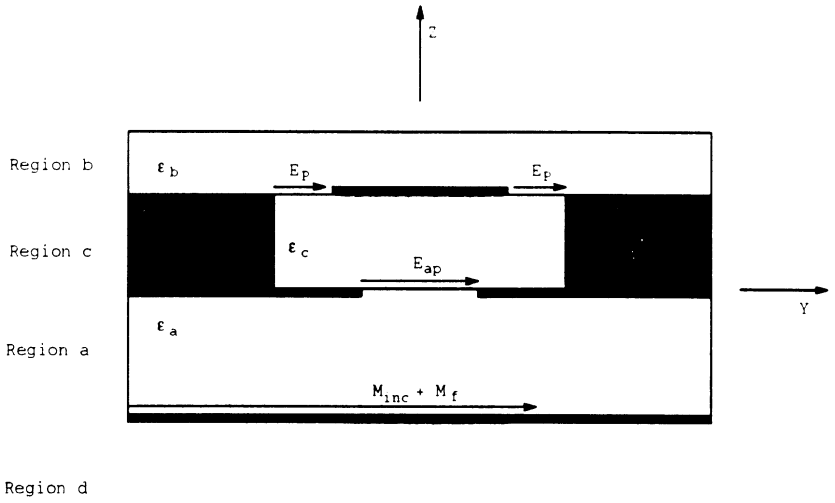

Figure 6: The schematic of the original problem.

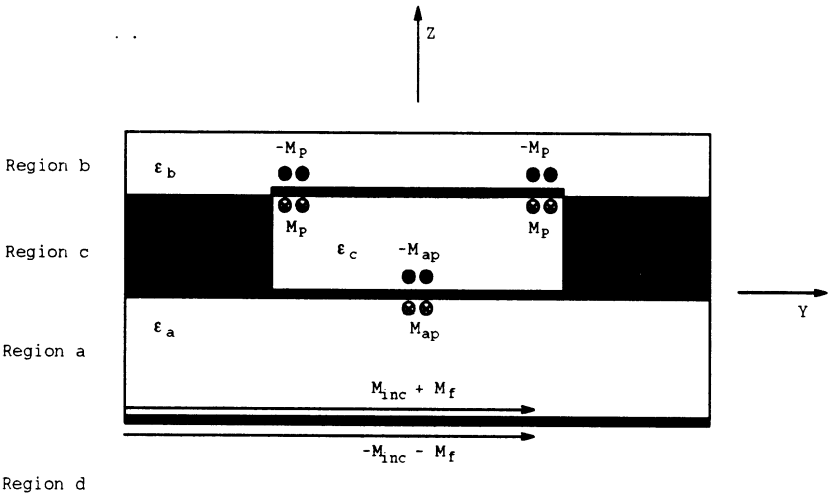

Figure 7: The equivalent problem after closing the opening above the cavity and slot by conductor. Suitable magnetic currents are added to ensure the equivalence.

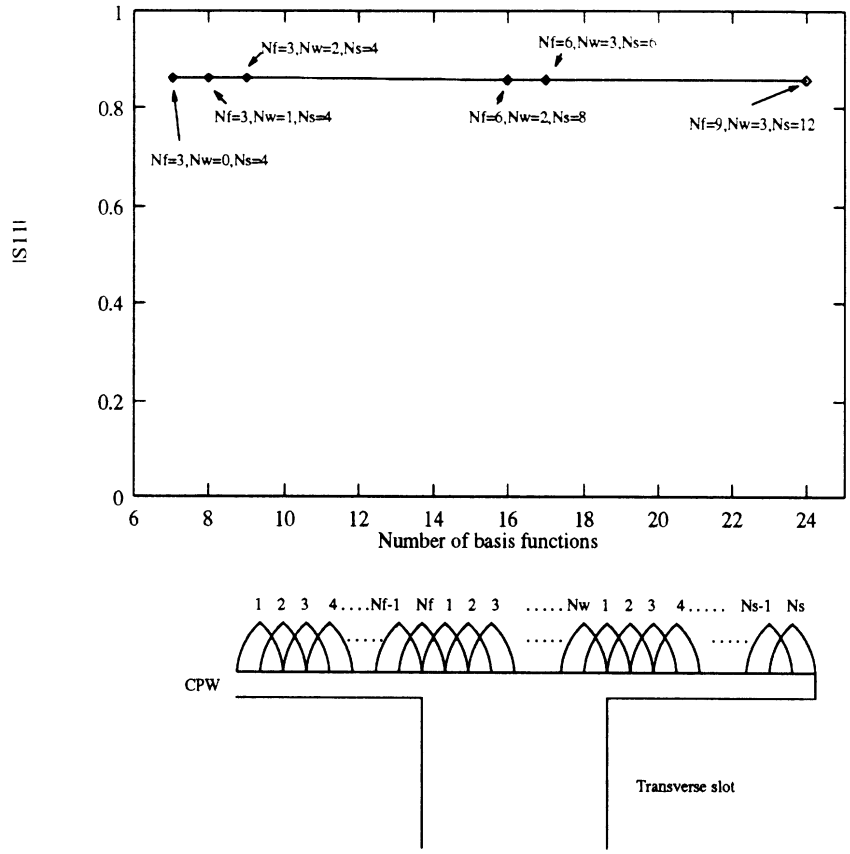

Figure 8: The amplitude of $|S_{11}|$ v.s. number of basis functions on the CPW. N_f, N_w and N_s are as shown in figure. 5 PWS modes are used on the patch, 3 on the transverse slot, 5 on the aperture. The PWS modes on the CPW extends from the end to 3/4 wavelength. The traveling wave mode extends 3 wavelengths.

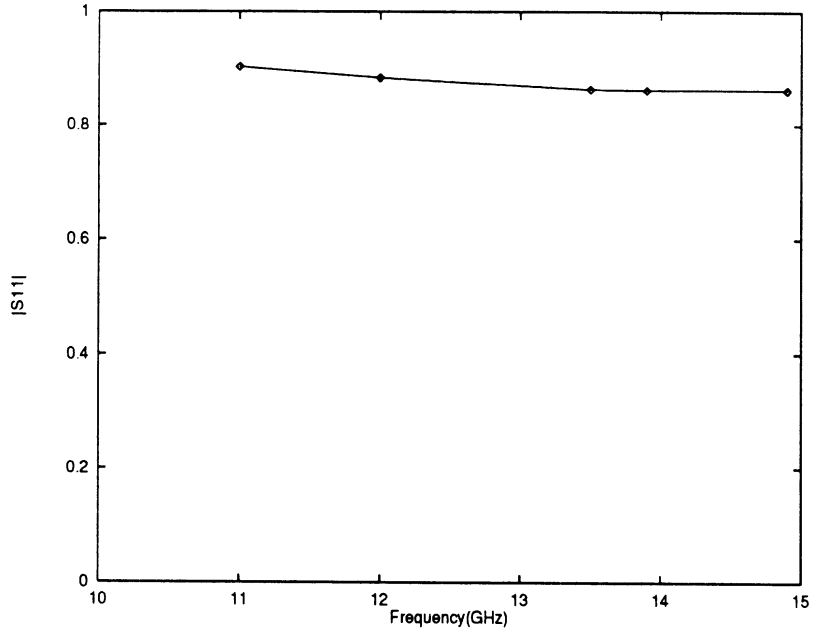

Figure 9: The amplitude of $|S_{11}|$ v.s. frequency. N_f, N_w and N_s are 3, 0 and 4 respectively. Other parameters are the same as Fig. 8.